RESEARCH

Experimental investigation of the effect of bioinspired flow field design on polymer electrolyte membrane fuel cell

Sadiq T. Bunyan[1] · Hayder A. Dhahad[2] · Dhamyaa S. Khudhur[3] · Talal Yusaf[4] · Steve Hall[4]

Abstract
Flow fields are a primary component of polymer electrolyte membrane fuel cells (PEMFCs), the components supplying fuel cells with reactant gases, such as hydrogen and oxygen. However, the flow fields of fuel cells are limited by the nonuniform poor distribution of reactant gases, unintended pressure drop across channels, and poor water management, among other issues. Thus, relevant designs must focus on obtaining the lowest possible pressure drop while attaining the best possible distribution of reactant gases, further improving cell performance. In this work, the impact of novel bioinspired flow field designs on PEMFC performance was investigated. Three flow field configurations, namely, sunflower-inspired flow field (SUFF), flower of life-inspired flow field (FLFF), and palm frond-inspired flow field (PAFF), were designed, as inspired by the shape of the sunflower (i.e., flower of life and palm frond). Results revealed that the optimal operating conditions for the fuel cell were 1 L/min and 1.1 bar. The bioinspired configurations significantly affected PEMFC performance at a low voltage (< 0.645 V), but the impact was negligible at a high voltage (> 0.645 V). Furthermore, the ohmic loss region and the concentration loss region were both significantly improved by the bioinspired designs. The maximum power density was significantly increased for SUFF, FLFF, PAFF1, and PAFF2 by 16.84%, 6.07%, 6.32%, and 10.40%, respectively.

Keywords Fuel cell · Bipolar plate · Flow field · Flow channel · Bioinspired

✉ Sadiq T. Bunyan
newsadiq1993@gmail.com

Hayder A. Dhahad
Hayder.A.Dhahad@uotechnology.edu.iq

Dhamyaa S. Khudhur
damiaamech@uomustansiriyah.edu.iq

Talal Yusaf
t.yusaf@cqu.edu.au

Steve Hall
s.hall@cqu.edu.au

[1]   Ministry of Higher Education and Scientific Research, Baghdad, Iraq

[2]   Mechanical Engineering Department, University of Technology, Baghdad, Iraq

[3]   Mechanical Engineering Department, Mustansiriyah University, Baghdad, Iraq

[4]   School of Engineering and Technologies, Central Queensland University, Queensland, Australia

Introduction

Environmental pollution caused by the rampant use of fossil fuels is considered a persistent global problem [1]. The depletion of fossil fuel stocks is another issue [2]. Consequently, clean energy production has become crucial and urgent [3], with fuel cells becoming widely available for this purpose. Fuel cells operate analogously to batteries except that the former do not require recharging [4]. Among many fuel cell types, the polymer electrolyte membrane (PEM) is the most desired because of its high electrical efficiency and uncomplicated design [5, 6]. Its design parameters, such as membrane electrode assembly, flow channels, endplates, and current collectors, are used for water and thermal management and control of polymer electrolyte membrane fuel cell (PEMFC) performance [7, 8]. The generation of cathode water is also influenced by this flow field design. In particular, flow channels are used to effectively maintain water at a proper level and subsequently control flooding, hotspots, and dehydration, further avoiding a decrease in cell performance. Past studies have focused on improving flow channel design to similarly enhance PEMFC performance. Straight-flow

channels have been investigated through different modifications, such as channel blockage, channel traps, and ribbed flow channels [9–11]. The serpentine flow field (SFF) has also been modified using sinusoidal wavy channels, multipass channels, and porous inserts in channels [12–18] to enhance water management and cell power performance. Similarly, the parallel flow field has also undergone modifications, such as by using single- and double-in/out mechanisms for parallel flow fields, micro-distributor channels, and Z-type, U-type, U–Z-type, and zigzag channels, to prevent the maldistribution of reactants, achieve acceptable current distribution, and increase cell power [19–28]. Meanwhile, nature-inspired flow field configurations, such as lung-, tree-, and leaf-inspired designs, have been investigated to enhance the output power of PEMFCs [29–39]. Unconventional flow fields have also been tested on fuel cells to uniformly distribute the reactant and current by using honeycomb-, blood vessel-, and cuttlefish-inspired designs and intersect–flow channels [40–42]. Baffles (plain nickel foam) have been positioned in parallel flow channels where the channels and ribs on the cathode side have been entirely superseded, and the porosity of nickel metal foam was 80%. The concentrations of oxygen were increased by the inclusion of the metal foam. Also, the high porosity value for metal foam led to improved current density [43]. Porous carbon inserts were placed with a uniform arrangement and staggered arrangement in the serpentine flow channel to improve PEMFC performance and liquid water management, where water was taken up by the porous inserts and transported to channels via the lateral sides after passing through the interfacial area of the GDL and rib [44]. The PEMFC with a three-dimensional fine-mesh flow field was thoroughly examined, and the distribution of liquid water in the three-dimensional flow field was qualitatively analyzed. It has been encountered that the 3-D fine mesh design can aid in removing liquid water from PEMFCs while particularly enhancing the supply of the reactants from the channels to electrodes [45]. In other work, three configurations inspired by the Fibonacci sequence were investigated. The Fibonacci-inspired configurations enhance the peak power density and current density. Furthermore, the ohmic losses region has been enhanced with the Fibonacci design [46]. Also, parallel configuration and serpentine configuration have been merged to obtain a hybrid design. This design improves the performance of fuel cell by achieving a uniform distribution of gas, temperature, and current. But it produces high pressure drop [47]. Many flow field designs were meticulously reviewed and classified into a multitude of different types, showcasing a comprehensive analysis of the impact of the configuration, dimensions, and geometric characteristics of the flow channel on the performance of the fuel cell [48]. On this basis, novel flow field configurations inspired by the shape of the sunflower, flower of life, and palm frond called sunflower-inspired flow field
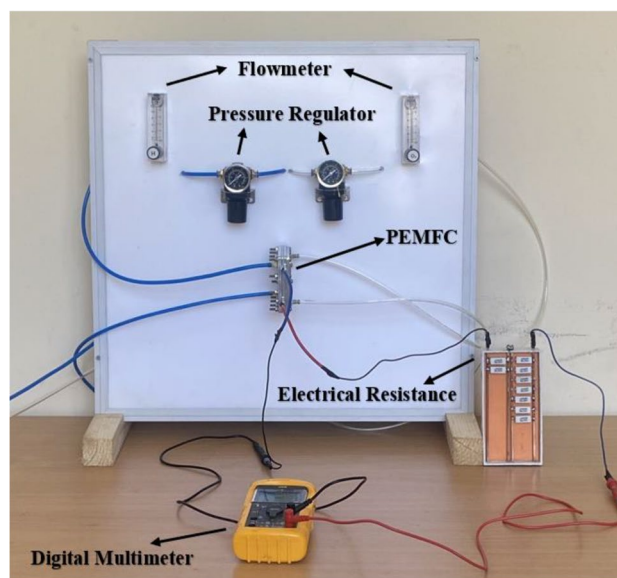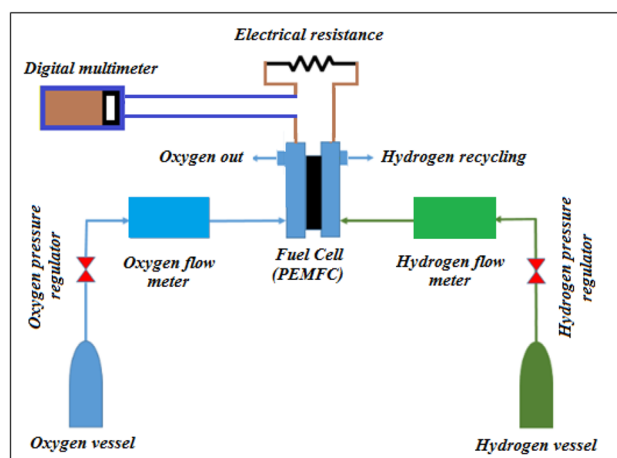

Fig. 1 Test apparatus

Fig. 2 Diagram of the test apparatus

(SUFF), flower of life-inspired flow field (FLFF), and palm frond-inspired flow field (PAFF), respectively, are recommended in this study.

Experimental setup

The test apparatus was composed of a PEMFC, oxygen and hydrogen vessels, a digital multimeter, pressure gauges, pipelines, flow meters, pressure regulators, and several electrical resistors (Fig. 1). The parts of the test apparatus are shown in Fig. 2. The type of fuel cell used in this study was PEM, which operates on oxygen and hydrogen (model: HEM-15, DuPont), with a weight of 0.4 kg. The PEMFC is shown in Fig. 3. The

size of the cell components is listed in Table 1. Both oxygen and hydrogen vessels were installed with a pressure gauge for discharging pressure gases. The purity level of the oxygen and hydrogen gases was 99%. Two pressure regulators for hydrogen and oxygen mounted on the test panel were used to control the pressure of gases entering the PEMFC, thus preventing membrane rupture; they were also used to calibrate pressure gauges. The hydrogen and oxygen gas flow that entered the PEMFC was measured using a single-phase flow and nonpulsating rotameter. The rotameter was lightweight and intuitive to read, with an accuracy of $\pm 6\%$, a working temperature of 55 ℃, and a working pressure of 0.4 MPa. The flow meter was mounted vertically on the test panel to achieve precise readings and adapted to the required flow rate by using a control valve. Then, a multimeter was utilized to measure different electrical properties. The multimeter was operated manually, with a relative humidity of 75%, a maximum reading of 3999, and an operating temperature range from 0 to 40 °C. Resistors were utilized to adjust the current of the PEMFC by varying its load. Then, different electrical resistors were connected in parallel and in series to obtain various resistance values. In particular, ceramic cement resistors with specifications of 0.22 Ω, 5 W, 24 g, and $\pm 5\%$ tolerance were used. The seated pipes were completely deflated prior to their connection and operation with the fuel cells. Practical experiments were executed to investigate the effects of varying pressures and flow rates on the performance of fuel cell and obtain the optimum operating conditions. The obtained optimal operating conditions were subsequently utilized to examine the effect of flow fields within the fuel cell with various loads.

Table 1 Component size of the PEMFC

Parameters	Values	Units
Endplate length	87	mm
Endplate thickness	5	mm
Endplate width	87	mm
Bipolar plate thickness	2	mm
Channel width	2	mm
Channel height	1	mm
Rib width	2.5	mm

the catalyst layer and flow channels, were identified. Then, the bioinspired configurations were drawn onto the bipolar plates. The engineering configurations of the different flow fields were designed using SolidWorks. In the second stage, the designs were exported to HSM-Works for creating G-codes, and the results were inputted into the CNC machine. The C-TEK CNC milling machine used in this study could complete the entire process of groove processing, milling, and drilling (Fig. 4). In particular, the CNC milling machine was used to fabricate the bipolar plates and drill the flow channels. In the last stage, the fabricated aluminum plate was manually cleaned, and all filings were removed. Aluminum with a density of 2500 kg/m³ was used to fabricate the bipolar plate because of its corrosion resistance, light weight, ease of manufacturability, thin-plate structure, and sufficient electrical and thermal conductivity [49]. The following four bioinspired designs of flow fields were developed and fabricated in addition to the basic SFF: SUFF, FLFF, PAFF1, and PAFF2.

Flow field design and manufacturing

The steps of designing and manufacturing the different flow fields can be described as follows: in the first stage, the dimensions and shapes of the selected elements, namely,
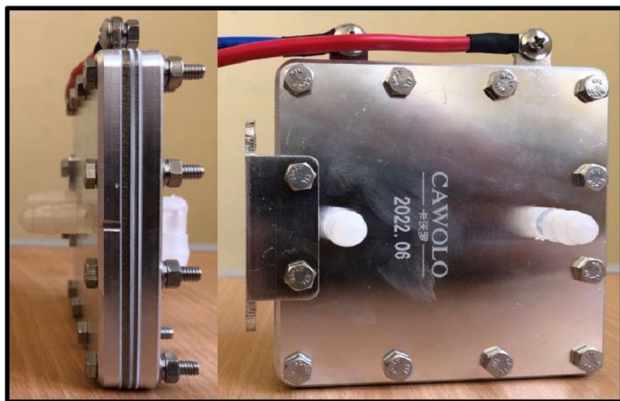

Fig. 3 PEMFC

Fig. 4 C-TEK CNC milling machine

The SFF is a widely used design for flow fields in PEMFCs. Thus, this conventional design was used for comparison with the novel bioinspired flow field configurations proposed in this experimental study. In terms of design, the SFF has a long and continuous channel, with a width of 2 mm, a depth of 1 mm, and a rib width of approximately 2.5 mm. The outlet and inlet diameters of the flow field plate were 5 mm. Figure 5 shows the design of the SFF before and after manufacturing based on the dimensional diagram. The constructal law, a fundamental principle in physics, demonstrates the notion that flow systems experience a continuous process of evolution, optimizing their designs to facilitate improved access for the currents that traverse them. The phenomena of design generation and development exemplify as natural mechanisms that aim to improve the pathways through which the currents flow [50]. Accordingly, bioinspired flow field configurations have been designed. Sunflower is a common plant; it has a peg root and a cylindrical unbranched stem covered with numerous fluffs, as shown in Fig. 6. On the basis of the fluff shape of the sunflower head, a flow channel (SUFF) was designed. This design consisted of an entrance with a diameter of 5 mm that was connected to 12 straight channels with a width of 1.18 mm distributed in all directions regularly. Then, the channels were connected to a grid with a width of 1 mm. The outlet diameter was 5 mm. The design resembling the sunflower flower is shown in Fig. 7. The flower of life has been regarded as a geometric symbol that includes a primary large circle with overlapping circles [51], such as that shown in Fig. 8. On the basis of the flower life shape, the flower life flow channel was designed (i.e., FLFF, Fig. 9). Here, the hexagonal part was cut out and designed in the form of flow channels with an inlet and outlet of 2.5 mm. The main channel was divided into two secondary channels by a rib with two sharply tapered ends. The width of the secondary channel was 2 mm, and the inlet and outlet

Fig. 6 Sunflower (*Helianthus annuus*)

diameters were 5 mm. The diameter of the external circle was 58.6. Palm fronds are the branched leaves of palm trees; they have a feathery shape and a rough texture. Palm fronds differ from tree leaves in that the former are separated from each other (Fig. 10). On the basis of the frond shape, flow channels (i.e., PAFF) were designed in this study. In particular, two different types of flow fields (i.e., PAFF1 and PAFF2) were developed. The first design had a straight main channel with a width of 2 mm connected to branch channels, while the second design had a tapered main channel connected to branch channels. The width of the starting point of the channel was 3.87 mm, gradually narrowing until it reached a width of 2.35 mm. The width of the subchannels in both types was 2 mm, and the width of the rib was 2 mm. The inlet and outlet diameters of the two designs were 5 mm. The diameter of the external circle was 58.6. Figures 11 and 12 show the PAFF1 and PAFF2 designs, respectively.
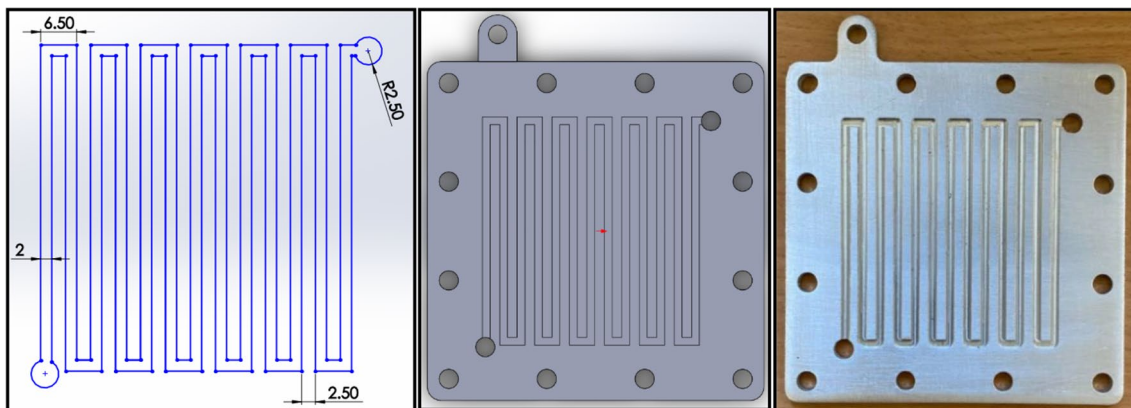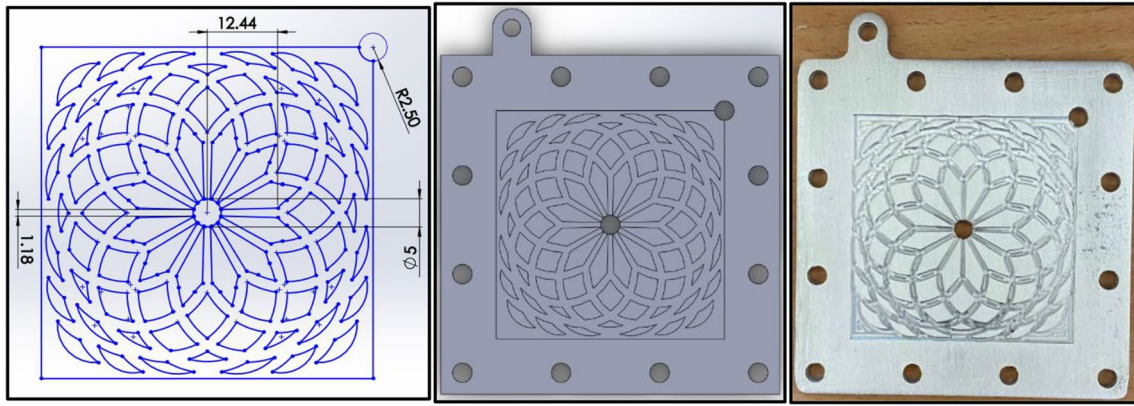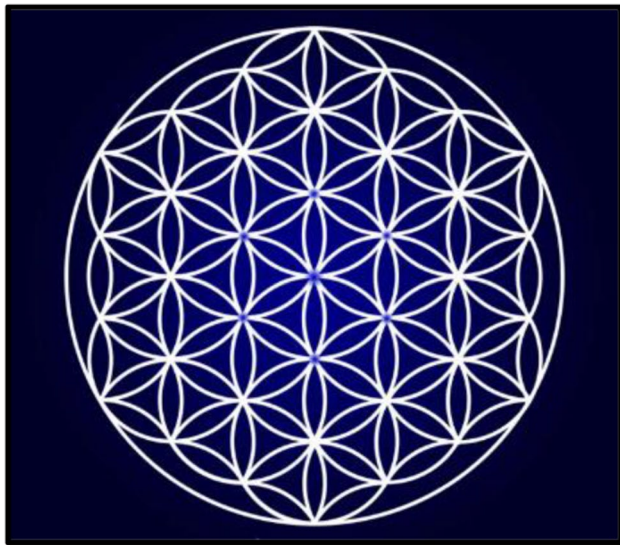

Fig. 5 SFF

Fig. 7 SUFF

Fig. 8 Sketch of flower life

Design and manufacture of endplates

Inlet and outlet holes were drilled into the endplates to match their corresponding holes in the previously manufactured flow fields while the endplates were being built. In the first step, the engineering details of the different endplates were drawn in SolidWorks. Then, for the purpose of generating G-codes, the endplate drawings were inputted into HSM-Works. Finally, the resulting G-codes were inputted into the C-TEK CNC milling machine for fabrication. The last stage entailed manually cleaning the endplate and removing any filings. The designed endplate was constructed from aluminum (Fig. 13). Gaskets were manufactured on the basis of the configurations and dimensions of the endplates and flow channels mentioned above. In general, gaskets in PEMFCs provide insulation and prevent leakages. Here, the gaskets were created using the commonly manufactured plastic material
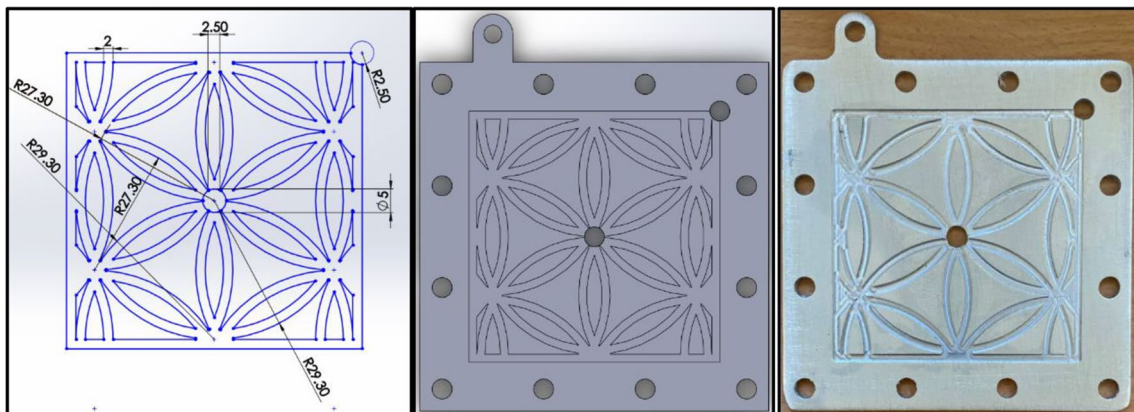

Fig. 9 FLFF

Fig. 10 Palm frond

polyethylene. The gasket used in this study is shown in Fig. 14.

Results and discussion

The experimental results were executed to investigate the effects of varying pressures and flow rates on fuel cell performance and obtain the optimum operating conditions. The relationship between current density and hydrogen flow rate at 0.1 Ω and 1 bar is demonstrated in Fig. 15. The results indicate that the increase in current density is proportional to the hydrogen flow rate until it approaches 1 L/min, where the increase in current density is insignificant. The empirical correlations between the current density and hydrogen flow rate of PEMFC are obtained by applying the progression analysis. The generated equation for SFF is the polynomial Eq. 4th order for the optimal curve fitting.

$$I = 3.2576\,\dot{m}4 - 12.005\,\dot{m}3 + 15.955\,\dot{m}2 - 8.8845\,\dot{m} + 2.0478 \tag{1}$$

$$\frac{dI}{d\,\dot{m}} = 13.0304\,\dot{m}^3 - 36.015\,\dot{m}^2 + 31.91\,\dot{m} - 8.8845 \tag{2}$$

At maximum current density $(\frac{dI}{d\,\dot{m}} = 0)$

$$13.0304\,\dot{m}^3 - 36.015\,\dot{m}^2 + 31.91\,\dot{m} - 8.8845 = 0$$

$\dot{m} = 1.150$ L/min

$I = 0.370 A/cm2$ *maximum current density*

The highest level of current density attainable for SFF is 0.370 A/cm^2 when the flow rate is at 1.150 L/min. Furthermore, a set of empirical correlations were developed by applying identical methodologies on the other designs, as outlined in Table 2, while maintaining identical pressure and resistance conditions. The utilization of the PAFF2 design resulted in the attainment of the highest current density for the PEM fuel cell. This outcome was due to the augmentation of the active area, which consequently led to an increase in the flow rate. As a result, the current density experienced a corresponding increase. Additionally, another contributing factor to this achievement is the effective distribution of hydrogen throughout the flow channels. The anticipated explanation for the increase in current density is that increasing the amount of hydrogen leads to an augmentation in the electrons released from the catalyst layer at
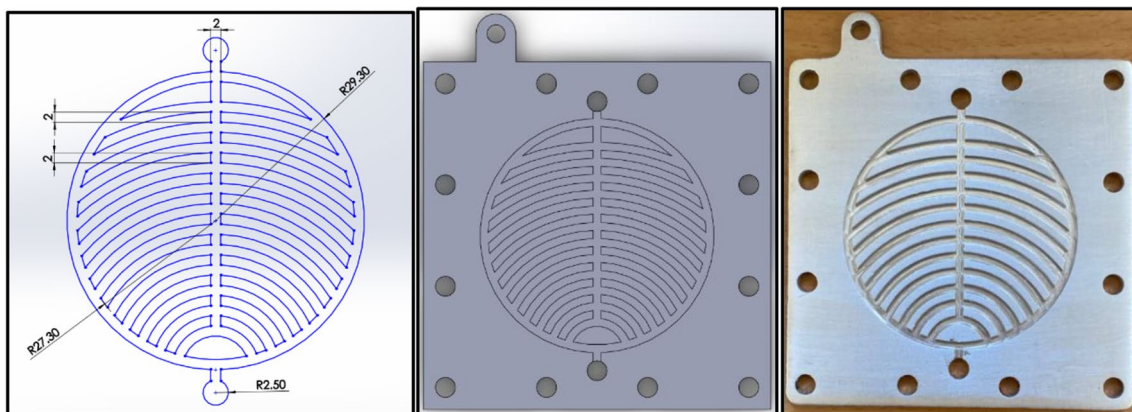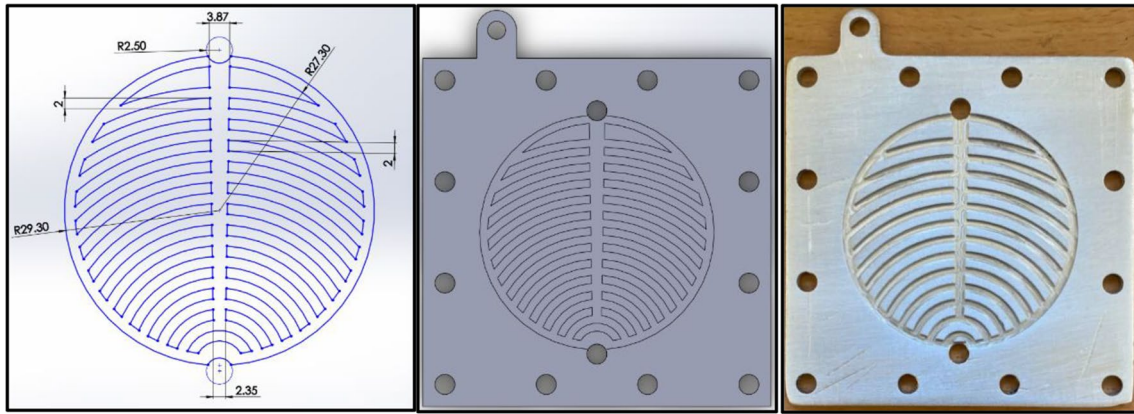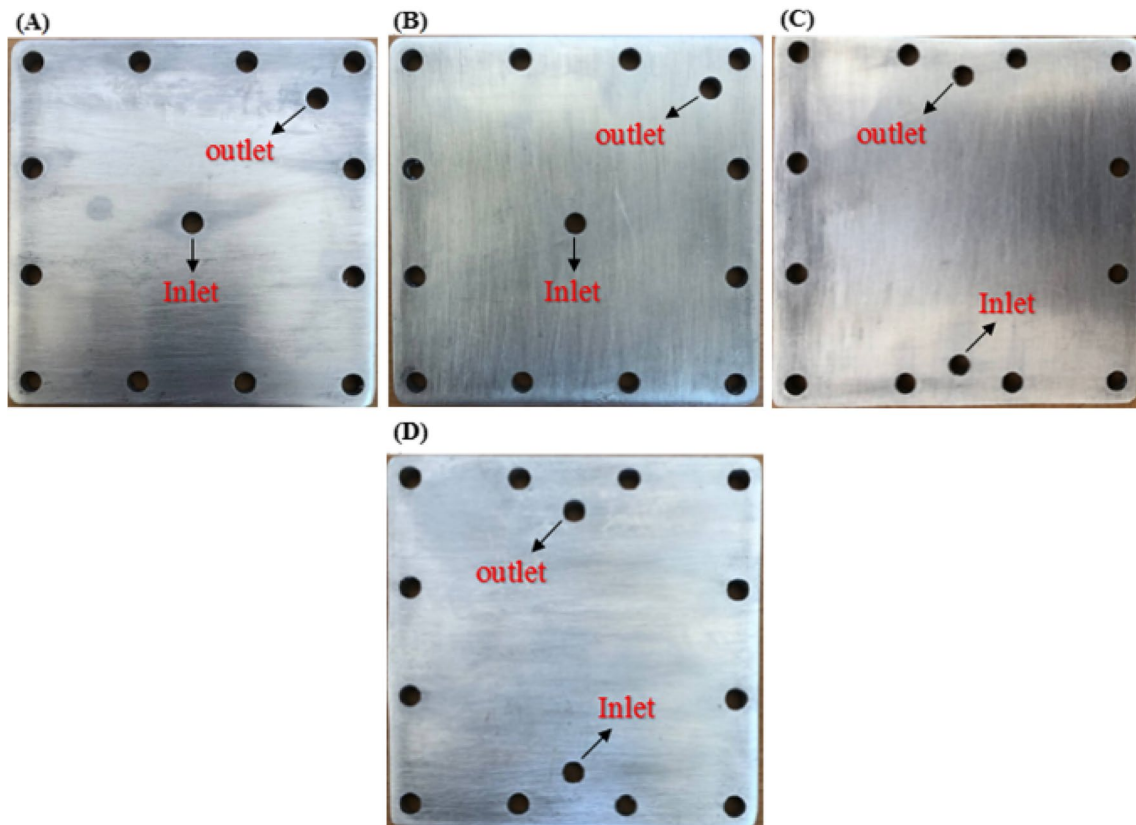

Fig. 11 PAFF1

Fig. 12 PAFF2

Fig. 13 Endplates for **A** SUFF, **B** FLFF1, **C** PAFF1, and **D** PAFF2

the anode. Thus, it increases until it reaches a maximum value. The maximum current density value depends on the active area limited by each flow channel design.

Figure 16 illustrates the relationship between the hydrogen pressure and voltage generated from PEM fuel cell at 1 L/min for different flow field designs. The findings suggest that the rise in voltage in a fuel cell is directly related to the hydrogen

pressure until it reaches a value of approximately 1.1 bar, at which point the increase in voltage becomes marginal. The empirical correlations between the voltage and hydrogen pressure of (PEMFC) for used configurations are obtained through the application of progression analysis. The equation generated for the (SFF) is a sixth-order polynomial equation, which ensures optimal curve fitting.
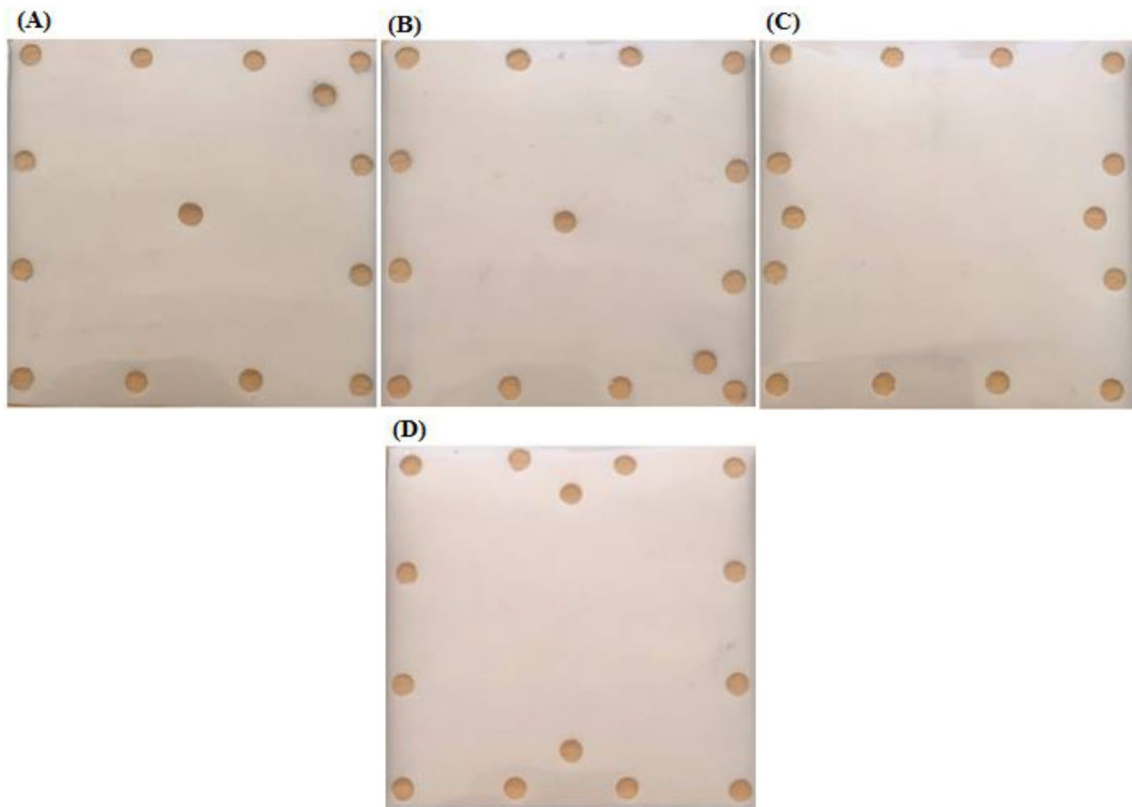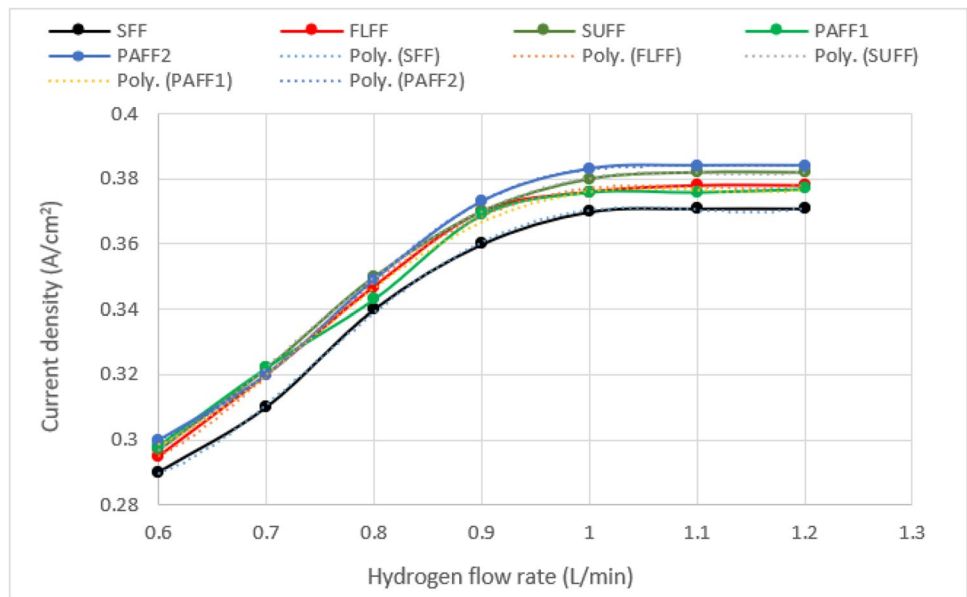
Fig. 14 Gaskets for **A** SUFF, **B** FLFF1, **C** PAFF1, and **D** PAFF2

Fig. 15 The relationship between current density and flow rate

Table 2 The empirical correlations of current

Design	Empirical correlation	$\dot{m}_H$ (L/min)	I max (A/cm^2)
SFF	$I = 3.2576\,\dot{m}^4 - 12.005\,\dot{m}^3 + 15.955\,\dot{m}^2 - 8.8845\,\dot{m} + 2.0478 \dots (1)$	1.150	0.370
FLFF	$I = -1.6667\,\dot{m}^5 + 10.379\,\dot{m}^4 - 23.78\,\dot{m}^3 + 25.302\,\dot{m}^2 - 12.411\,\dot{m} + 2.5537 \dots (3)$	1.146	0.377
SUFF	$I = 2.2348\,\dot{m}^4 - 8.1843\,\dot{m}^3 + 10.695\,\dot{m}^2 - 5.7256\,\dot{m} + 1.3603 \dots (4)$	1.156	0.381
PAFF1	$I = 2.7273\,\dot{m}^4 - 10.04\,\dot{m}^3 + 13.286\,\dot{m}^2 - 7.3194\,\dot{m} + 1.7223 \dots (5)$	1.156	0.376
PAFF2	$I = -27.778\,\dot{m}^6 + 149.17\,\dot{m}^5 - 326.53\,\dot{m}^4 + 371.96\,\dot{m}^3 - 232.18\,\dot{m}^2 + 75.47\,\dot{m} - 9.725 \dots (6)$	1.201	0.392

Fig. 16 The relationship between the pressure and voltage
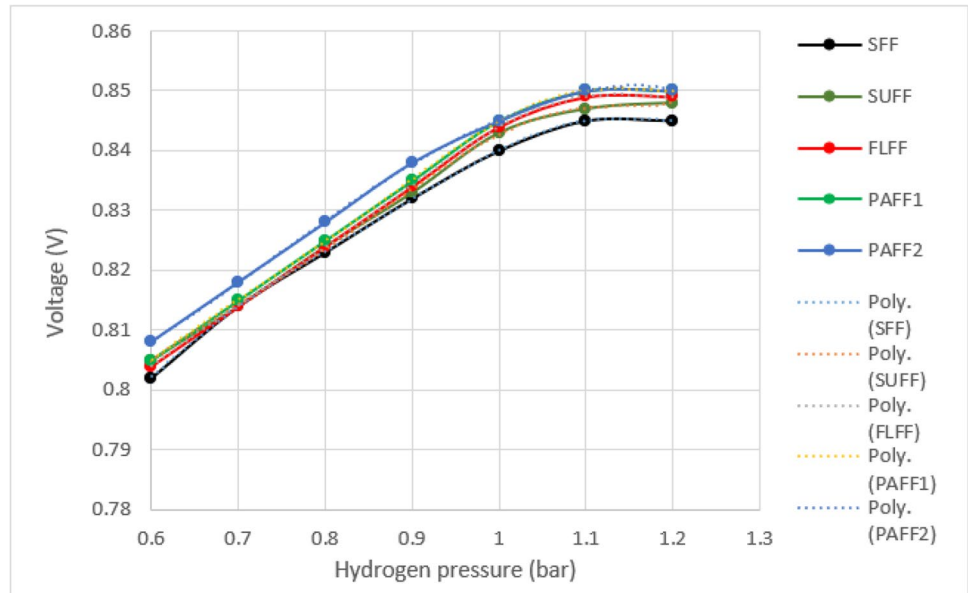
$$V = 7.6389P6 - 39.824P5 + 84.754P4 - 94.224P3 + 57.63P2 - 18.247P + 3.112 \tag{3}$$

$$\frac{dV}{dP} = 45.8334P^5 - 199.12P^4 + 339.016P^3 - 282.672P^2 + 115.26P - 18.24 \tag{4}$$

At maximum voltage $\left(\dfrac{dV}{dP} = 0 \right)$

$$45.8334P^5 - 199.12P^4 + 339.016P^3 - 282.672P^2 + 115.26P - 18.247 = 0$$

P = 1.136 bar
V = 0.84496 V maximum voltage

The maximum achievable voltage value for SFF reaches 0.844 V at 1.136 bar. Moreover, a set of empirical correlations was formulated through the application of identical methodologies on other configurations, as explicitly depicted in Table 3. The utilization of the PAFF2 design resulted in

Table 3 The empirical correlations of voltage

Design	Empirical correlation	P (bar)	V max (V)
SFF	$V = 7.6389P^6 - 39.824P^5 + 84.754P^4 - 94.224P^3 + 57.63P^2 - 18.247P + 3.112 \dots (7)$	1.136	0.84496
FLFF	$V = 6.9444P^6 - 35.096P^5 + 72.249P^4 - 77.625x^3 + 45.939P^2 - 14.106P + 2.538 \dots (9)$	1.20	0. 8487
SUFF	$V = 6.9444P^6 - 34.135P^5 + 68.162P^4 - 70.784P^3 + 40.307P^2 - 11.831P + 2.1788 \dots (10)$	1.167	0. 8464
PAFF1	$V = 6.9444P^6 - 35.096P^5 + 72.249P^4 - 77.625x^3 + 45.939P^2 - 14.106P + 2.539 \dots (11)$	1.20	0. 8487
PAFF2	$V = -3.4722P^6 + 17.933P^5 - 38.072P^4 + 42.328P^3 - 25.922P^2 + 8.3799P - 0.329 \dots (12)$	1.1586	0. 8517

the achievement of the highest voltage for the PEM fuel cell. The expected reason for the increase in voltage of the fuel cell is that increasing pressure reduces the activation energy, which in turn leads to a decrease in voltage loss. However, the increase in cell voltage is limited because the activation energy depends primarily on the type of catalyst.

Thus, the operating conditions used in the experiments to test the bioinspired configurations on the PEMFC and contrast them with the SFF configuration were 1 L/min and 1.1 bar. Figure 17 shows the polarization curve of the basic SFF design with respect to the SUFF design in terms of current density and voltage. In general, the current density increased

as the voltage decreased at a constant pressure and flow rate because of the ohmic losses in the PEMFCs. The polarization curve also presents three regions for concentration loss, ohmic loss, and activation loss. The activation loss region was negligibly affected by the SUFF design. The voltages required to reach the activation energy and start the reaction for SFF and SUFF were 0.185 and 0.182 V, respectively. The ohmic loss curve is divided into two regions. The voltage increased marginally in the first region and then crossed over to the other region at 0.645 V. This phenomenon corresponded to a significant increase in voltage as the pressure decreased further on the anode side. Meanwhile, the current

Fig. 17 Polarization curve of SUFF
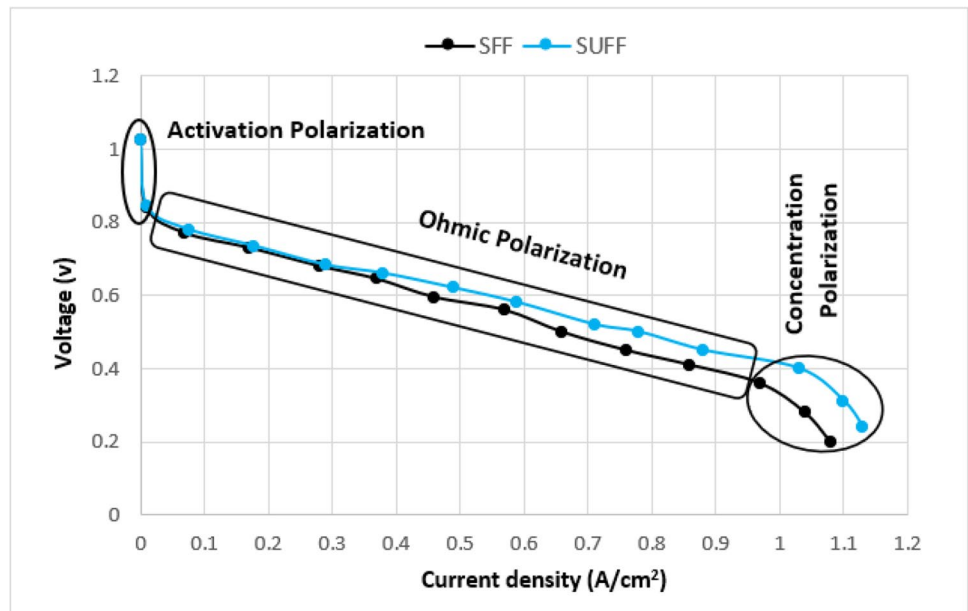
Fig. 18 Power curve of SUFF
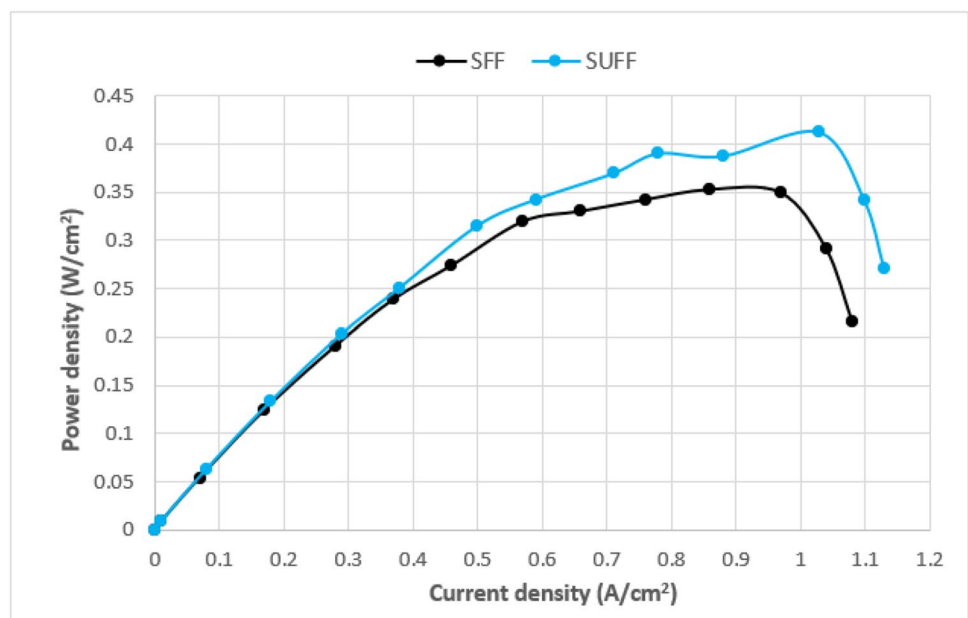
density in the concentration polarization region improved owing to the enhanced water management at the cathode side. In this area where the SUFF design was adopted, the concentration polarization for the SFF and SUFF designs started at 0.97 and 1.03 A/cm², respectively. The maximum current densities observed for the PEMFC in the SFF and SUFF designs were 1.08 and 1.13 A/cm², respectively. Figure 18 presents the power curves of the basic SFF and SUFF designs in terms of the current and power densities. The results confirm the higher power of the PEMFC for the SUFF design compared with the SFF design. The maximum power densities of the PEMFCs with the SUFF and SFF

designs were 0.412 and 0.3526 W/cm² at 1.03 and 0.86 A/cm², respectively. The improvement in peak power density with the SUFF design was 16.84%. The design of the flow field, inspired by the sunflower, matches the pin flow field design which decreases the pressure drop [48], with some positive differences in SUFF design that led to uniform distribution in reactants. Figure 19 shows the polarization curves of the FLFF and basic SFF designs. The FLFF design clearly influenced the polarization at voltages of < 0.645 V, but the impact was much less at > 0.645 V. Therefore, the activation loss region was marginally enhanced by the FLFF design. The voltage losses in the SFF and FLFF designs
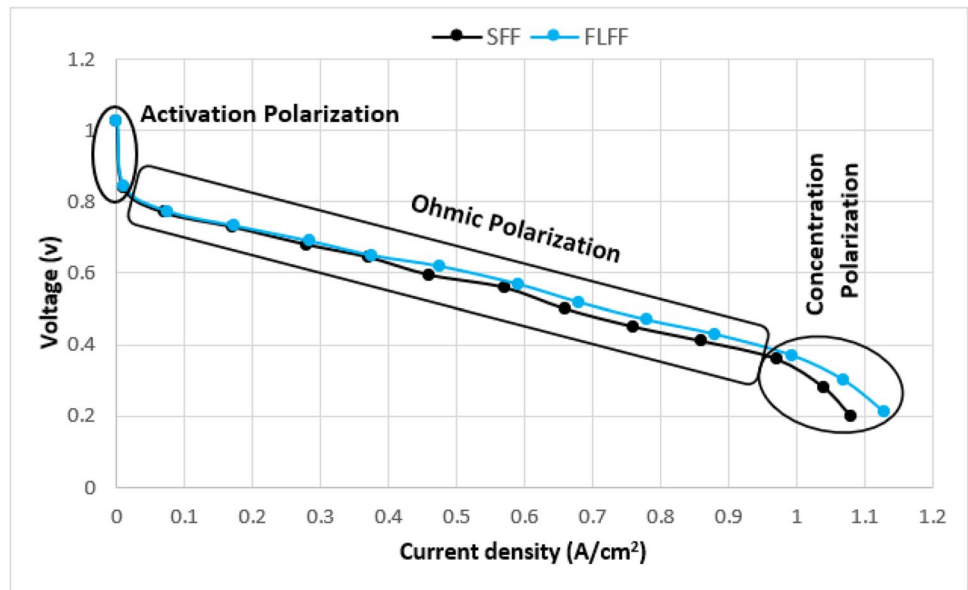

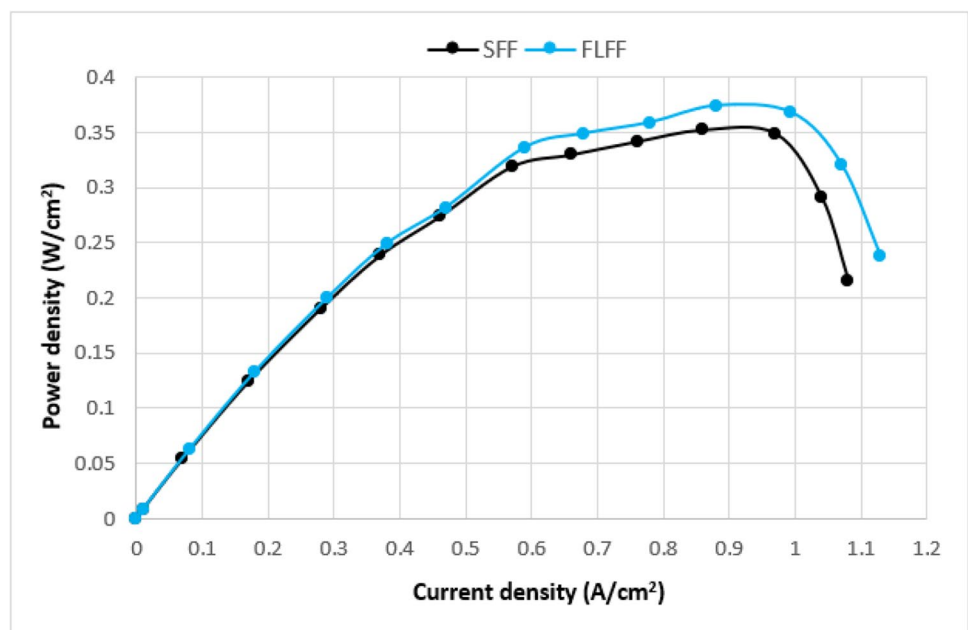**Fig. 19** Polarization curve of FLFF


Fig. 20 Power curve of FLFF

were 0.185 and 0.181 V, respectively. By contrast, the FLFF design resulted in significant enhancement of both voltage and current in the ohmic loss region compared with the basic SFF design, which indicates decreasing pressure at the anode side of the FLFF. Additionally, the concentration loss region achieved a considerable improvement in the current density, which indicates better water management at the cathode side of the FLFF design. The concentration loss regions for the SFF and FLFF designs corresponded to 0.97 and 0.994 A/cm^2, respectively. Meanwhile, the maximum current densities of the PEMFCs with the SFF and FLFF designs were 1.08 and 1.13 A/cm^2, respectively. Figure 20 shows the power curves of the FLFF and basic SFF designs.

The FLFF design produced a higher cell power than the SFF design. The maximum power densities of the FLFF and SFF designs were 0.374 and 0.3526 W/cm^2 at 0.88 and 0.86 A/cm^2, respectively. Therefore, the enhancement of peak power for the FLFF design was 6.07%. The main reason for the superiority of the flower of life flow field is that the active area of FLFF is larger than that of SFF and the streamlined design in the FLFF channels reduces pressure drop. Figure 21 shows a comparison of the polarization curves of the PAFF and basic SFF designs. The voltage losses in the activation polarization region for both PAFF designs were 0.005 V lower than that for the SFF design. Given the further reduced pressure drops at the anode sides

Fig. 21 Polarization curves of PAFF1 and PAFF2
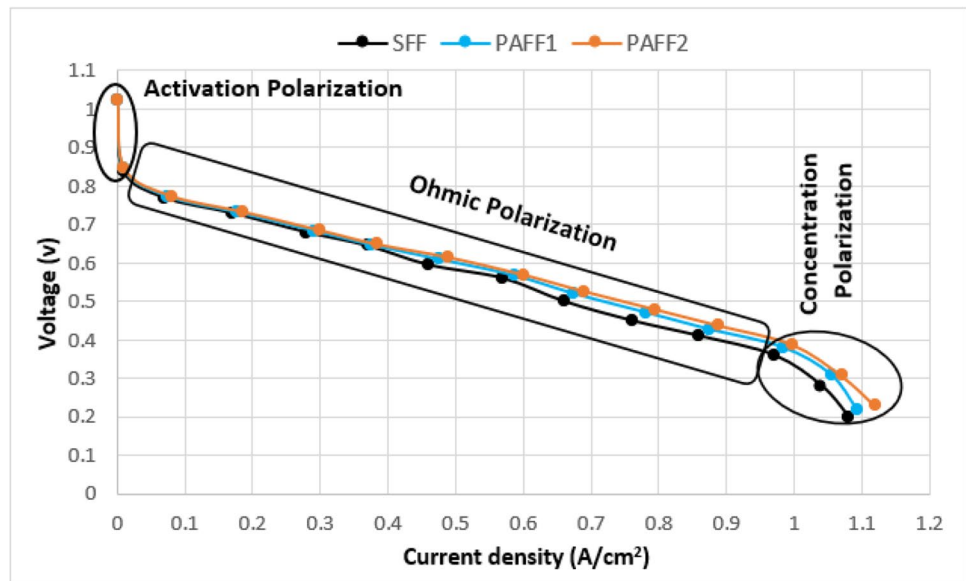
Fig. 22 Power curves of PAFF1 and PAFF2
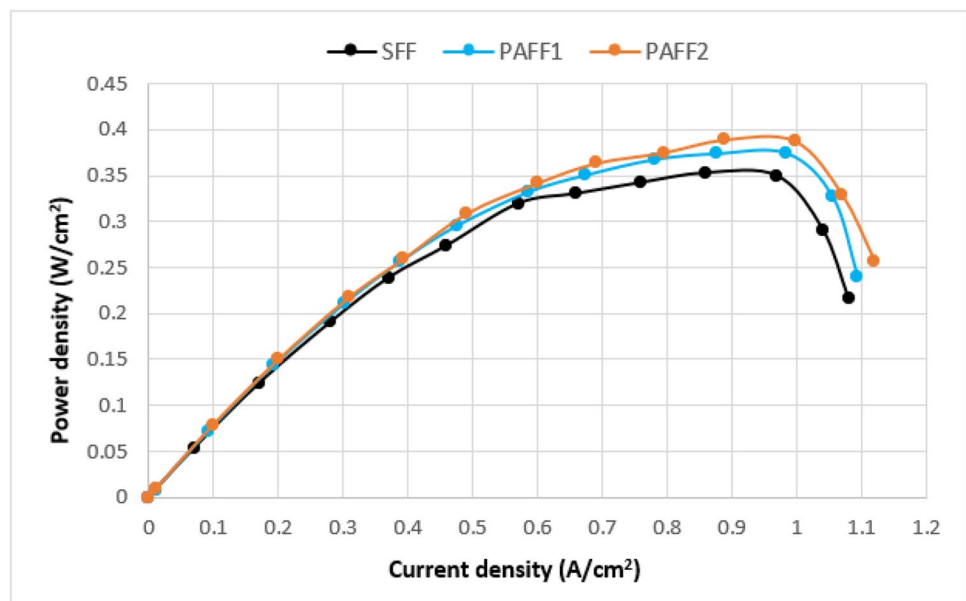
of the PAFF designs, the voltage in the ohmic loss region was higher than that of the SFF design. Additionally, the reduction in mass transport losses at the cathode side of the PAFF designs improved the current density in the concentration polarization region. The concentration losses of the SFF, PAFF1, and PAFF2 designs were 0.97, 0.984, and 0.997 A/cm^2, respectively. The maximum current densities of the PEMFCs with the SFF, PAFF1, and PAFF2 designs were 1.08, 1.093, and 1.12 A/cm^2, respectively. The power curve trends indicate that the power produced by the PEMFC with the PAFF designs is higher than that of PEMFC with the SFF design (Fig. 22). The maximum power densities of the PEMFCs with the SFF, PAFF1, and PAFF2 designs were 0.3526, 0.3749, and 0.3893 W/cm^2 at 0.86, 0.984, and 0.889 A/cm^2, respectively. The percentage increases in the maximum powers of PAFF1 and PAFF2 were 6.32% and 10.40%, respectively. It is expected that the distinguishing characteristic contributing to the improved performance of the PAFF2 design in comparison to the PAFF1 design lies in the inclusion of a main tapered channel within the second configuration. This feature performs to force the reactants to flow into the adjacent subchannels gradually, thereby facilitating the complete occupation of the empty channels which provides a uniform distribution of the reactants. Overall, the proposed bioinspired flow field design improved the performance of the fuel cell.

In the realm of these findings, there is a significant point to dissect: the marked increase in fuel cell performance owing to the adoption of the bioinspired designs. This increment can be primarily attributed to the unique characteristics of the bioinspired designs, specifically their design nature that emulates the geometric progression. The design of these flow fields influences the distribution of reactant gases within the fuel cell, leading to the observed improvements in performance. Beginning with the activation polarization region, a minor improvement was seen with the utilization of bioinspired designs. While this might seem trivial, even a minute enhancement in this region can have consequential benefits. This is because activation polarization losses originate from the inherent resistance to initiating the electrochemical reactions that produce power in the fuel cell. Thus, a reduction in these losses implies that these reactions can start more readily, leading to improved power output at the lower end of the current–voltage curve. Going to the ohmic polarization region, the implementation of bioinspired designs led to a notable improvement. The enhanced voltage, revealing a decreased pressure drop at the anode side of the bioinspired configurations, can be construed as the result of an optimized gas flow pathway. This optimized pathway is an outcome of decreased flow resistance, and the individual spiral structure, thus undervaluing the energy losses associated with the movement of reactants through the fuel cell. Additionally, the improvement in the current density

of the concentration region across all novel configurations reveals an enhancement in water management at the cathode side. This is important since sufficient management of generated water in PEM fuel cells is challenging. A suboptimal removal of generated water can restrain oxygen passes to the catalyst sites, thereby decreasing the performance of the fuel cell. Thus, this enhancement can lead to a considerable elevation in performance at the higher end of the polarization curve. It is also worth noting the substantial improvements in peak power densities that were reached with the bioinspired configurations, which demonstrated the best performance. This result indicates that the geometric design principles, inspired by the structure of Palm fronds and flower of life, can be reliant to engineer optimal flow channels for PEMFC. It is evidence of the possibility of nature-inspired design techniques in the field of energy systems. The enhancements imply that additional investigation and refinement of these configurations may ultimately result in fuel cells with even greater efficiency and performance.

Conclusion

The experimental results were executed to investigate the effects of varying pressures and flow rates on fuel cell performance. The results indicate that the increase in current density is proportional to the hydrogen flow rate until it approaches 1 L/min, where the increase in current density is insignificant. The highest level of current density attainable for SFF is 0.370 A/cm^2 when the flow rate is at 1.150 L/min. Also, the findings indicate that the rise in voltage in a fuel cell is directly related to the hydrogen pressure until it reaches a value of approximately 1.1 bar, at which point the increase in voltage becomes marginal. The maximum achievable voltage value for SFF reaches 0.844 V at 1.136 bar. So, the experiments were conducted with optimal operating conditions to examine novel designs of flow channels which were 1 L/min and 1.1 bar. The bioinspired designs considerably impact PEMFC performance at low voltages (lower than 0.645 V), while the influence is minor at high voltages (higher than 0.645 V). The bioinspired configurations narrowly positively affected the activation loss region of the PEM fuel cell. Meanwhile, the ohmic loss region and the concentration loss region were significantly enhanced by the bioinspired designs. The concentration loss regions of the SUFF, FLFF, PAFF1, and PAFF2 started at 1.03, 0.994, 0.984, and 0.997 A/cm^2 compared with 0.97 A/cm^2 for SFF. Furthermore, the maximum power density increased significantly by 16.84%, 6.07%, 6.32%, and 10.40% for SUFF, FLFF, PAFF1, and PAFF2, respectively. The SUFF design attained the best performance and was considered the optimal design.

Author contribution Conceptualization, T.Y. and H.A.D.; methodology, S.T.B.; software, S.T.B.; validation, S.T.B.; formal analysis, H.A.D.; investigation, S.T.B.; resources, S.T.B.; data curation, S.T.B.; writing—original draft preparation, H.A.D.; writing—review and editing, S.H. supervision, H.A.D.; project administration, D.S.K. All authors have read and agreed to the published version of the manuscript.

Data availability No datasets were generated or analyzed during the current study.

Declarations

Competing interests The authors declare no competing interests.

References

1. Dhahad HA, Chaichan MT (2020) The impact of adding nano-Al2O3 and nano-ZnO to Iraqi diesel fuel in terms of compression ignition engines' performance and emitted pollutants. Therm Sci Eng Prog 18:100535

2. Höök M, Tang X (2013) Depletion of fossil fuels and anthropogenic climate change—a review. Energy Policy 52:797–809

3. Lund PD et al (2015) Review of energy system flexibility measures to enable high levels of variable renewable electricity. Renew Sustain Energy Rev 45:785–807

4. Rajashekara K (2000) Propulsion system strategies for fuel cell vehicles. Citeseer

5. Albarbar A, Alrweq M (2017) Proton exchange membrane fuel cells: design, modelling and performance assessment techniques. Springer

6. Babu ARV, Kumar PM, Rao GS (2018) Parametric study of the proton exchange membrane fuel cell for investigation of enhanced performance used in fuel cell vehicles. Alex Eng J 57(4):3953–3958

7. Kumar MM, Karthikeyan P, Kumar A (2016) Influence of temperature and pressure on the performance of proton exchange membrane fuel cell. Asian J Res Soc Sci Humanit 6(5):1387–1400

8. Karthikeyan P et al (2013) Optimization of operating and design parameters on proton exchange membrane fuel cell by using Taguchi method. Procedia Eng 64:409–418

9. Kumar PM, Kolar AK (2010) Effect of cathode design on the performance of an air-breathing PEM fuel cell. Int J Hydrogen Energy 35(2):671–681

10. Ramin F, Sadeghifar H, Torkavannejad A (2019) Flow field plates with trap-shape channels to enhance power density of polymer electrolyte membrane fuel cells. Int J Heat Mass Transf 129:1151–1160

11. Cai G et al (2020) Design and optimization of bio-inspired wave-like channel for a PEM fuel cell applying genetic algorithm. Energy 192:116670

12. Jeon D et al (2008) The effect of serpentine flow-field designs on PEM fuel cell performance. Int J Hydrogen Energy 33(3):1052–1066

13. Muthukumar M et al (2014) Performance studies on PEM Fuel cell with 2, 3 and 4 pass serpentine flow field designs. Appl Mech Mater 592:1728–1732

14. Shimpalee S, Greenway S, Van Zee J (2006) The impact of channel path length on PEMFC flow-field design. J Power Sources 160(1):398–406

15. Dhahad HA, Alawee WH, Hassan AK (2019) Experimental study of the effect of flow field design to PEM fuel cells performance. Renew Energy Focus 30:71–77

16. Seyhan M et al (2017) Performance prediction of PEM fuel cell with wavy serpentine flow channel by using artificial neural network. Int J Hydrogen Energy 42(40):25619–25629

17. Karthikeyan P, Vasanth R, Muthukumar M (2015) Experimental investigation on uniform and zigzag positioned porous inserts on the rib surface of cathode flow channel for performance enhancement in PEMFC. Int J Hydrogen Energy 40(13):4641–4648

18. Pal V, Karthikeyan P, Anand R (2015) Performance enhancement of the proton exchange membrane fuel cell using pin type flow channel with porous inserts. J Power Energy Eng 3(05):1

19. Maharudrayya S, Jayanti S, Deshpande A (2006) Pressure drop and flow distribution in multiple parallel-channel configurations used in proton-exchange membrane fuel cell stacks. J Power Sources 157(1):358–367

20. Hossain MS, Shabani B, Cheung CP (2017) Enhanced gas flow uniformity across parallel channel cathode flow field of proton exchange membrane fuel cells. Int J Hydrogen Energy 42(8):5272–5283

21. Lim B et al (2017) Numerical analysis of modified parallel flow field designs for fuel cells. Int J Hydrogen Energy 42(14):9210–9218

22. Lim B et al (2020) Numerical investigation of the effect of three-dimensional modified parallel flow field designs on proton exchange membrane fuel cell performance. Chem Eng Sci 217:115499

23. Ghanbarian A, Kermani MJ (2016) Enhancement of PEM fuel cell performance by flow channel indentation. Energy Convers Manage 110:356–366

24. Azarafza A et al (2019) Comparative study of conventional and unconventional designs of cathode flow fields in PEM fuel cell. Renew Sustain Energy Rev 116:109420

25. Wang X et al (2020) Numerical and experimental investigation of baffle plate arrangement on proton exchange membrane fuel cell performance. J Power Sources 457:228034

26. Liu H et al (2018) Numerical analysis of parallel flow fields improved by micro-distributor in proton exchange membrane fuel cells. Energy Convers Manag 176:99–109

27. Afshari E, Ziaei-Rad M, Dehkordi MM (2017) Numerical investigation on a novel zigzag-shaped flow channel design for cooling plates of PEM fuel cells. J Energy Inst 90(5):752–763

28. Roshandel R, Arbabi F, Moghaddam GK (2012) Simulation of an innovative flow-field design based on a bio inspired pattern for PEM fuel cells. Renew Energy 41:86–95

29. Kloess JP et al (2009) Investigation of bio-inspired flow channel designs for bipolar plates in proton exchange membrane fuel cells. J Power Sources 188(1):132–140

30. Guo N, Leu MC, Koylu UO (2014) Bio-inspired flow field designs for polymer electrolyte membrane fuel cells. Int J Hydrogen Energy 39(36):21185–21195

31. Damian-Ascencio CE et al (2017) Numerical modeling of a proton exchange membrane fuel cell with tree-like flow field channels based on an entropy generation analysis. Energy 133:306–316

32. Senn S, Poulikakos D (2004) Laminar mixing, heat transfer and pressure drop in tree-like microchannel nets and their application for thermal management in polymer electrolyte fuel cells. J Power Sources 130(1–2):178–191

33. Cheng SJ, Miao JM, Tai CH (2012) Numerical simulation applied to study the effects of fractal tree-liked network channel designs on PEMFC performance. Adv Mater Res 488:1219–1223

34. Ozden A et al (2017) Designing, modeling and performance investigation of bio-inspired flow field based DMFCs. Int J Energy Res 42(33):21546–21558

35. Asadzade M, Shamloo A (2017) Design and simulation of a novel bipolar plate based on lung-shaped bio-inspired flow pattern for PEM fuel cell. Int J Energy Res 41(12):1730–1739

36. Trogadas P et al (2018) A lung-inspired approach to scalable and robust fuel cell design. Energy Environ Sci 11(1):136–143

37. Ghadhban SA, Alawee WH, Dhahad HA (2021) Study effects of bio-inspired flow filed design on polymer electrolyte membrane fuel cell performance. Case Stud Therm Eng 24:100841

38. Zhang S et al (2022) Performance of proton exchange membrane fuel cells with honeycomb-like flow channel design. Energy 239:122102

39. Wang CT, Chang CP, Shaw CK, Cheng JY (2009) Fuel Cell Bionic Flow Slab Design. ASME J Fuel Cell Sci Technol 7(1):011009

40. Wang C-T, Hu Y-C, Zheng P-L (2010) Novel biometric flow slab design for improvement of PEMFC performance. Appl Energy 87(4):1366–1375

41. Kuo J-K (2007) The effects of buoyancy on the performance of a PEM fuel cell with a wave-like gas flow channel design by numerical investigation. Int J Heat Mass Transf 50(21–22):4166–4179

42. Dong-Hui W et al (2017) A novel intersectant flow field of metal bipolar plate for proton exchange membrane fuel cell. Int J Energy Res 41(14):2184–2193

43. Afshari E, Mosharaf-Dehkordi M, Rajabian H (2017) An investigation of the PEM fuel cells performance with partially restricted cathode flow channels and metal foam as a flow distributor. Energy 118:705–715

44. Palaniswamy K, Marappan M, Jothi VR (2016) Influence of porous carbon inserts on scaling up studies for performance enhancement on PEMFC. Int J Hydrogen Energy 41(4):2867–2874

45. Zhang G et al (2018) Multi-phase simulation of proton exchange membrane fuel cell with 3D fine mesh flow field. Int J Energy Res 42(15):4697–4709

46. Bunyan ST et al (2023) Effect of a novel flow field design on PEM fuel cell performance. In: 2023 16th International Conference on Developments in eSystems Engineering (DeSE). IEEE pp 156–161

47. Limjeerajarus N, Santiprasertkul T (2020) Novel hybrid serpentine-interdigitated flow field with multi-inlets and outlets of gas flow channels for PEFC applications. Int J Hydrogen Energy 45(25):13601–13611

48. Bunyan ST et al (2023) The effect of flow field design parameters on the performance of PEMFC: a review. Sustainability 15(13):10389

49. Brett DJ, Brandon NP (2007) Review of materials and characterization methods for polymer electrolyte fuel cell flow-field plates. J Fuel Cell Sci Technol 4:29–44

50. Bejan A, Zane JP (2012) Design in nature: the law of physics that guides the development of organisms is the same for inanimate nature and engineered systems. Mech Eng-CIME 134(6):42–48

51. Melchizedek D (1999) The ancient secret of the flower of life, vol 1. Light Technology Publishing